Differences in Hemodynamics and Rupture Rate of Aneurysms at the Bifurcation of the Basilar and Internal Carotid Arteries

R. Doddasomayajula, B. Chung, F. Hamzei-Sichani, C.M. Putman, and J.R. Cebral

ABSTRACT

BACKGROUND AND PURPOSE: Cerebral aneurysms in the posterior circulation are known to have a higher rupture risk than those in the anterior circulation. We sought to test the hypothesis that differences in hemodynamics can explain the difference in rupture rates.

MATERIALS AND METHODS: A total of 117 aneurysms, 63 at the tip of the basilar artery (27 ruptured, 36 unruptured, rupture rate = 43%) and 54 at the bifurcation of the internal carotid artery (11 ruptured, 43 unruptured, rupture rate = 20%) were analyzed with image-based computational fluid dynamics. Several hemodynamic variables were compared among aneurysms at each location and between ruptured and unruptured aneurysms at each location.

RESULTS: On average, aneurysms at the basilar tip had more concentrated inflow ($P < .001$), a larger inflow rate ($P < .001$), a larger maximum oscillatory shear index ($P = .003$), more complex flows ($P = .033$), and smaller areas under low wall shear stress ($P < .001$) than aneurysms at the bifurcation of the internal carotid artery. In general, ruptured aneurysms had larger inflow concentration ($P = .02$), larger shear concentration ($P = .02$), more complex flows ($P < .001$), and smaller minimum wall shear stress ($P = .003$) than unruptured aneurysms.

CONCLUSIONS: High flow conditions, characterized by large and concentrated inflow jets, complex and oscillatory flow patterns, and wall shear stress distributions with focalized regions of high shear and large regions of low shear, are associated with aneurysm rupture, especially for basilar tip aneurysms. The higher flow conditions in basilar tip aneurysms could explain their increased rupture risk compared with internal carotid bifurcation aneurysms.

ABBREVIATIONS: BAtip = basilar artery tip; corelen = core-line length; ICAbif = internal carotid artery bifurcation; ICI = inflow concentration index; LSA = areas under low wall shear stress; max = maximum; min = minimum; OSI = oscillatory shear index; Q = flow rate; SCI = shear concentration index; VE = mean velocity; WSS = wall shear stress

Intracranial aneurysms are balloon-like pathologic dilations of the cerebral blood vessel walls. An estimated 2%–5% of the general population is affected by intracranial aneurysms.[1] Rupture of intracranial aneurysms is an event associated with high mortality and disability rates; consequently, many physicians often preventively treat incidentally discovered aneurysms. However, the treatment risk can exceed the low natural risk of rupture of incidental aneurysms.[2,3] Therefore, it is important to precisely distinguish high-risk aneurysms for immediate treatment from low-risk aneurysms, which could be conservatively followed.

Several patient, demographic, and behavioral characteristics have been investigated as possible risk factors, including sex, age, family history, smoking, hypertension, and ethnicity. Past studies have indicated that in addition to the size of the aneurysm, location is an important risk factor for intracranial aneurysm rupture.[4] In particular, aneurysms in the posterior circulation have been shown to have an overall higher rupture risk than aneurysms in the anterior circulation. The cause of this difference in rupture risk is largely unknown.[5] Because aneurysm evolution is thought to be governed by a progressive degradation and weakening of the vessel wall in response to abnormal flow conditions,[6] it is logical to ask whether differences in aneurysm hemodynamics, induced by diverse configurations and geometries of vessels of the anterior and posterior circulations, could help explain the various rupture rates.

The purpose of this study was to test whether intrasaccular flow characteristics are different between aneurysms at the basilar

Hemodynamic and geometric variables used in the study and the aspect of the aneurysm they characterize

Variables	Metrics	Characterizes
Hemodynamics		
Q, ICI	Inflow rate, inflow concentration index	Inflow jet
VE, KE	Mean velocity, kinetic energy	Flow speed in aneurysm
VO, SR, VD	Vorticity, shear rate, viscous dissipation	Flow rotation deformation/dissipation in aneurysm
<WSS>, WSSmin, WSSmax, SCI, LSA	Mean, min, and max WSS, shear concentration index, area under low WSS	WSS distribution
<OSI>, OSImax	Mean, max oscillatory shear index	Oscillatory flow/WSS
Corelen	Length of vortex core lines	Flow complexity
Podent, podenum	POD entropy and number of modes	Flow stability
Geometry		
Aneurysym size, volume, area, SizeR	Aneurysm diameter, volume, area, size ratio	Aneurysm size
Neck size, area	Neck diameter, area	Neck size
Depth, aspect ratio	Aneurysm depth, aspect ratio	Aneurysm shape elongation
Artery, branch1, branch2	Diameter parent and branch arteries	Artery sizes
Symmetry	Ratio of branch diameters	Bifurcation symmetry
<Taper>, taper1, taper2	Mean taper, branch taper	Artery tapering

Note:—POD indicates proper orthogonal decomposition; SizeR, size ratio.

artery tip (BAtip) in the posterior circulation and the internal carotid artery bifurcation (ICAbif) in the anterior circulation, as well as between ruptured and unruptured aneurysms at these locations. These locations were selected because the BAtip is the most common location of intracranial aneurysm rupture in the posterior circulation[7] and is anatomically similar to the ICAbif in that they are both terminal bifurcations of a major feeding artery. The information generated in this study is useful for understanding what hemodynamic conditions predispose aneurysms to rupture and which mechanobiologic processes could be involved in aneurysm weakening and eventual rupture.

MATERIALS AND METHODS

Image and Patient Data

We have developed a data base of intracranial aneurysms imaged with 3D rotational angiography. This data base contains 3D rotational angiography images and anonymized clinical information, including rupture status, size, and location and patient sex and age of approximately 1800 intracranial aneurysms. All aneurysms from our data base located at either the BAtip or ICAbif were included in the study. A total of 117 aneurysms were studied, with the distribution of locations as follows: 63 BAtip aneurysms consisting of 27 ruptured and 36 unruptured with a rupture rate of 43%, and 54 ICAbif aneurysms, among which 11 were ruptured and 43 were unruptured, with a rupture rate of 20%. Among the 117 patients studied, there were 94 (80%) women and 23 (20%) men. There was no statistical difference between sexes in the BAtip and ICAbif aneurysms ($P = .8163$). The mean age of the ICAbif group was slightly younger (52 years) than that of the BAtip group (57 years) ($P = .0284$).

Vascular and Flow Modeling

Computational fluid dynamics models of all 117 aneurysms were constructed from the corresponding 3D rotational angiography images, by using a methodology previously developed.[8] Briefly, the 3D rotational angiography images were filtered to reduce noise and the vascular geometry was reconstructed with an iso-surface-deformable model.[9] These vascular models were subsequently smoothed, and the vessel branches were truncated at

planes orthogonal to their axes. The ICAbif models extended proximally to the cavernous ICA, and the BAtip, at least to the origin of the basilar artery; the models included both vertebral arteries if they were adequately depicted in the 3D rotational angiography images.

Numeric simulations based on 3D incompressible Navier-Stokes equations were performed on the 117 patient-specific aneurysm geometries by using pulsatile flow conditions. Because patient-specific flow information was unavailable, typical flow boundary conditions for a healthy subject derived from phase-contrast MR imaging (On-line Fig 1) were scaled with the inlet cross-sectional areas to achieve a mean wall shear stress (WSS) of 15 dynes/cm^2 prescribed at the inlets for all the models. Fully developed velocity profiles were prescribed at the inlets by using the Womersley solution.[10] Outflow boundary conditions were selected to produce flow divisions consistent with the Murray law to avoid unrealistic jumps in the wall shear stress from parent to daughter branches. Assumptions included Newtonian viscosity for blood and rigid vessel walls. The simulations had a minimum mesh resolution of 200 μm and a time resolution of 10 ms and were run for 2 cardiac cycles by using an in-house fully implicit finite-element solver.[11,12]

Flow variables such as the flow rate (Q), maximum wall shear stress (WSSmax), inflow concentration index (ICI), and the shear concentration index (SCI) were computed from the results of the second cycle to characterize the flow conditions within the aneurysms.[13,14] Geometric variables such as aneurysm size (Asize) and aspect ratio (AR) were computed from the 3D anatomic models. The definitions of vessel geometric variables are presented in On-line Fig 2. The Table presents a list of all the hemodynamic and geometric variables analyzed.
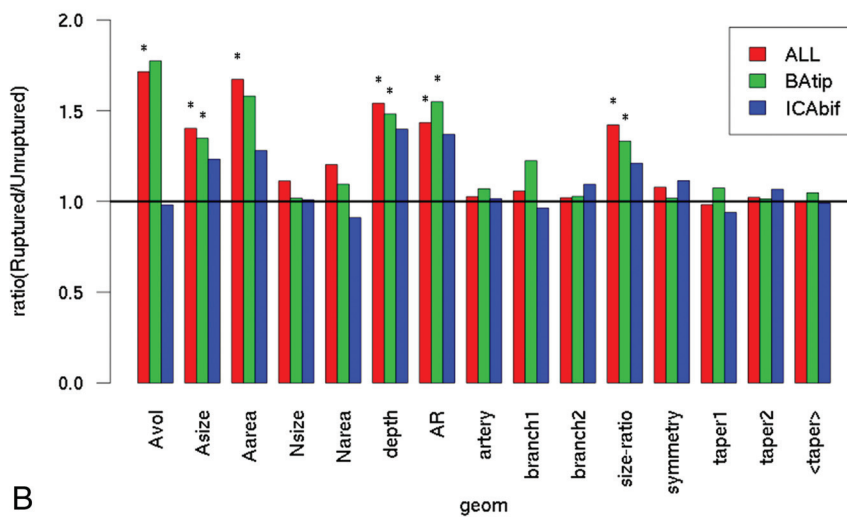
Data Analysis

The hemodynamic parameters listed in the Table were used to test the following: 1) whether aneurysms at the BAtip have different hemodynamic environments than those at the ICAbif, and 2) whether ruptured and unruptured aneurysms have different flow environments at each of these 2 locations. Two-sided Wilcoxon
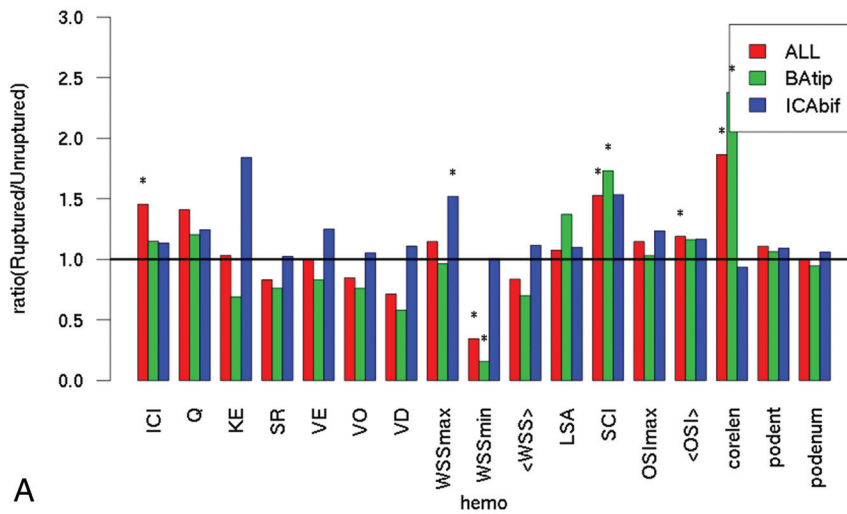
FIG 1. Ruptured-versus-unruptured aneurysms. Ratio of mean hemodynamic (*A*) and geometric (*B*) variables of ruptured over unruptured aneurysms for all aneurysms (*red bars*) and by location (*green bars*, BAtip; *blue bars*, ICAbif). *Asterisks* indicate statistically significant differences. Hemo indicates hemodynamic; geom indicates geometric; <taper>, mean taper; KE, kinetic energy; SR, shear rate; VO, vorticity; VD, viscous dissipation; <WSS>, mean WSS; podent, POD entropy; podenum, POD number of modes; <OSI>, mean OSI; A, aneurysm; N, neck; AR, aspect ratio.

rank sum tests were used to compare continuous variables between these groups. Differences were considered statistically significant with $P < .05$ (95% confidence level). To test for correlations or statistical dependence between the geometric and hemodynamic variables, we performed a Spearman rank correlation test among all the variables. A size-based comparison was then performed to assess any size-specific differences in ruptured and unruptured aneurysms at both locations. For this purpose, aneurysms were subdivided into 3 size groups: 1) large, >13 mm; 2) medium, 7–13 mm; and 3, small, <7 mm. Then the statistical analysis was repeated.[2]

RESULTS

The rupture rate among BAtip aneurysms was 43% compared with a 20% rupture rate in ICAbif aneurysms. A 2 × 2 contin-

gency table analysis based on the Fisher exact test confirmed a statistically significant association between the aneurysm location (BAtip or ICAbif) and rupture rate ($P = .0107$).

A comparison of hemodynamic and geometric variables between ruptured and unruptured aneurysms at both locations (red bars), along with similar comparisons for aneurysms at the BAtip (green bars) and at the ICAbif (blue bars), is shown in Fig 1 (data is provided in On-line Tables 1–3 as means and SDs for ruptured and unruptured aneurysms for all aneurysms and by location). The bars in these graphs indicate the ratio of mean values of the corresponding variables of ruptured aneurysms over the mean values of the unruptured aneurysms. Variables that are significantly different between these groups are marked by an asterisk.

In general, irrespective of the location, ruptured aneurysms had more concentrated inflow jets (ICI, $P = .02$), more concentrated WSS distributions (SCI, $P = .02$), more complex flow patterns (characterized by a longer vortex core-line length [corelen], $P < .0001$), and lower minimum WSS (WSSmin, $P = .003$) than unruptured aneurysms, as indicated in Fig 1A. Geometrically, ruptured aneurysms were larger (aneurysm volume, $P = .006$; aneurysm size, $P = .002$; aneurysm area, $P = .005$; size ratio, $P = .003$) and had more elongated shapes (depth, $P < .001$; aspect ratio, $P = .001$) than unruptured aneurysms (red bars in Fig 1B).

Similar associations were found for aneurysms located at the BAtip (green bars in Fig 1A). Specifically, ruptured BAtip aneurysms had higher WSS concentration (SCI, $P = .02$), more complex flow patterns (corelen, $P < .0001$), and lower minimum WSS ($P = .02$) than unruptured aneurysms at this location. Ruptured BAtip aneurysms were also larger (aneurysm size, $P = .02$; size ratio, $P = .03$) and more elongated (depth, $P = .01$; aspect ratio, $P = .001$) than unruptured BAtip aneurysms (green bars in Fig 1B). In contrast, ruptured ICAbif aneurysms had larger maximum WSS ($P = .03$) than unruptured ICAbif aneurysms (blue bars in Fig 1). All other hemodynamic or geometric variables did not reach statistical significance.

Hemodynamic and geometric characteristics of aneurysms (including both ruptured and unruptured aneurysms) located at the BAtip and the ICAbif are shown in Fig 2. In general, BAtip aneurysms had more concentrated inflow jets (ICI, $P < .001$), larger
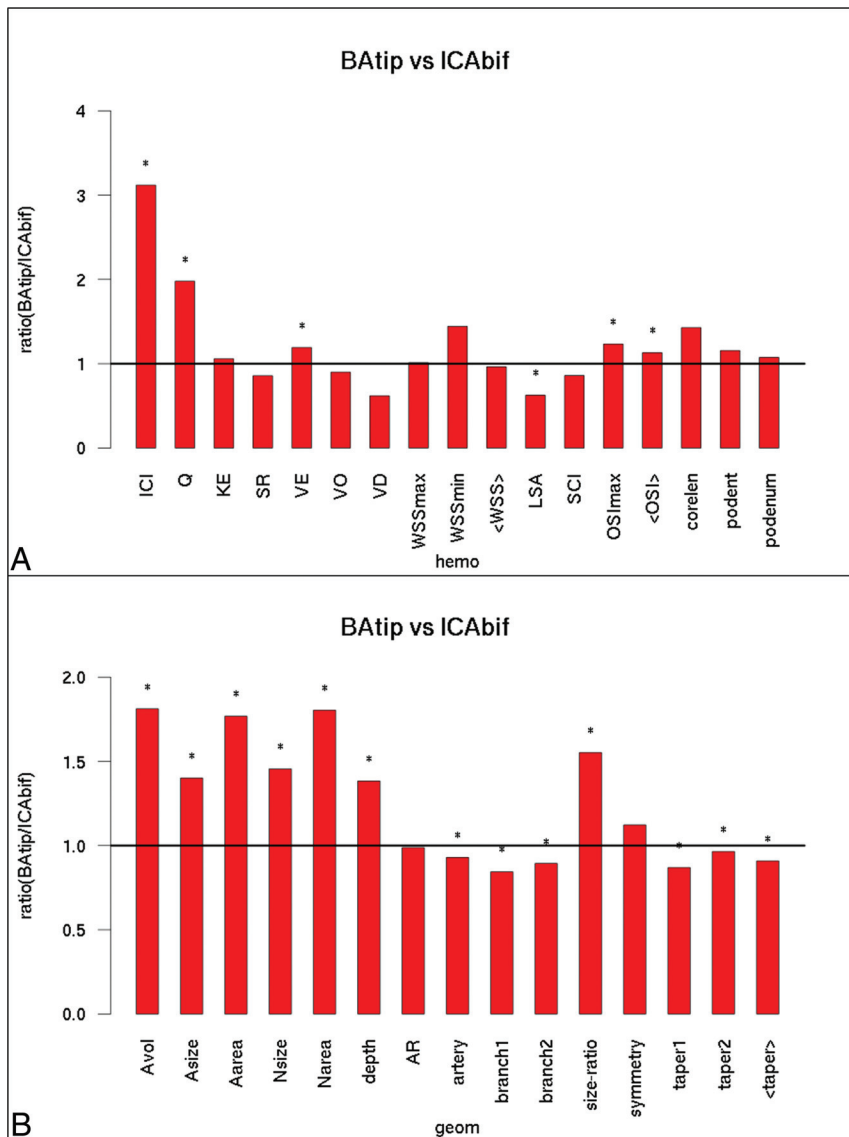
FIG 2. BAtip-versus-ICAbif aneurysms. Ratio of mean hemodynamic (A) and geometric (B) variables of BAtip aneurysms over ICAbif aneurysms. *Asterisks* indicate statistically significant differences. KE indicates kinetic energy; SR, shear rate; VO, vorticity; VD, viscous dissipation; <WSS>, mean WSS; podent, POD entropy; podenum, POD number of modes; <OSI>, mean OSI; hemo, hemodynamic; geom, geometric; <taper>, mean taper; A, aneurysm; N, neck; AR, aspect ratio.

inflow rates ($P < .001$; mean velocity [VE], $P = .04$), more oscillatory flows (maximum oscillatory shear index [OSImax], $P = .005$; mean OSI, $P = .04$), and smaller areas under low WSS (LSA, $P < .0001$) compared with ICAbif aneurysms. Additionally, BAtip aneurysms were larger (aneurysm volume, $P = .0005$; aneurysm size, $P = .0004$; Area, $P = .0006$; size ratio, $P < .001$) and had deeper domes (depth, $P = .01$) and wider necks (neck size, $P < .0001$; neck area, $P < .0001$) than ICAbif aneurysms. Most interesting, both parent and branch arteries were of a smaller caliber in the BAtip group (artery, $P = .003$; branch1, $P < .001$; branch2, $P = .006$) and had lower tapering (taper1, $P < .001$; taper2, $P = .04$; mean taper, $P = .0004$) compared with the ICAbif group.

The differences between BAtip and ICAbif hemodynamic environments were further analyzed by subdividing the aneurysms into groups based on their size (Fig 3). For large aneurysms (red bars), there were no significant differences in the hemodynamic variables. However, medium-sized BAtip aneurysms (green bars) had more concentrated inflow jets and higher inflow rates (ICI, $P < .001$; Q, $P = .003$), more oscillatory flows (OSImax, $P = .03$), and larger areas under low WSS ($P = .001$) compared with medium-sized ICAbif aneurysms. Similarly, small BAtip aneurysms had higher flow conditions characterized by larger inflow rates, more concentrated inflow jets, and larger intrasaccular velocity (ICI, $P < .001$; Q, $P = .01$; VE, $P = .04$) as well as larger areas under low WSS ($P < .001$) compared with small ICAbif aneurysms.

Illustrative examples of ruptured and unruptured aneurysms at the BAtip and ICAbif are shown in Figs 4 and 5, respectively. These figures show visualizations at peak systole of the WSS distribution, the inflow jets, the streamline patterns, and the flow structure by using vortex center lines. In both examples, the flow in the ruptured aneurysm (upper row) is characterized by a strong inflow jet impacting a concentrated area of the dome and producing a complex flow pattern within the aneurysm. In contrast, the unruptured aneurysms (lower row) exhibit a more uniform WSS distribution associated with a more diffuse inflow jet and simpler flow pattern.

DISCUSSION

Posterior circulation intracranial aneurysms are known to have higher rupture rates compared with anterior circulation intracranial aneurysms[15]; considering that there are 2 ICAs for every 1 basilar artery in a complete circle of Willis, the reported differences in rupture risk are probably even more substantial.[5] The results in our series showing a rupture rate of 43% among BAtip aneurysms compared with 20% among ICAbif aneurysms ($P = .0107$) are consistent with those published in previous studies.[5,15]

The exact reasons for these differences in rupture risks or the rupture mechanisms are still relatively unknown.[16] Thus, several previous studies have sought to determine the effects of morphometric features and hemodynamic forces on the mechanobiology of the vessel wall and on the rupture risk of intracranial aneurysms.[17-19] Some studies have suggested that aneurysms located at bifurcations are at the highest risk of rupture, attributing it to the increased hemodynamic stress at the tip of the bifurcation.[5,20] We sought to further understand the differences between these 2 locations by evaluating the intra-aneurysmal hemodynamics and

morphometric features of analogous bifurcations representing both systems.

Can et al[21] suggested that the larger P1-P1 angle of the BAtip bifurcation causes greater flow divergence into the daughter posterior cerebral arteries, thus causing lower WSS and leading to aneurysmal initiation. Our results do not seem to support the idea that this same mechanism results in aneurysm progression and rupture. Irrespective of whether the aneurysms were located at the BAtip or at the ICAbif, ruptured aneurysms in our series had more concentrated inflow jets, more concentrated WSS distributions, and longer vortex core-line lengths and, at the same time, had lower WSSmin. Although not confirmed in the ICAbif location, the BAtip location has significantly "higher flow conditions" associated with ruptured aneurysms compared with the unruptured ones. The longer vortex core-line lengths are an indicator of more complex flows and are consistent with the findings in several previously reported studies comparing ruptured and unruptured aneurysms.[14,22] Morphologically, ruptured aneurysms in our study were larger and more elongated than unruptured aneurysms as identified in multiple prior studies.[23,24]

Similarly, higher flow conditions were observed in general when comparing all BAtip and ICAbif aneurysms irrespective of rupture status. The differences observed between aneurysms at these locations were significant for small and medium-sized aneurysms, but not for large ones. This finding may be due to increased inertia effects associated with larger aneurysms.

Understanding the differences in the intra-aneurysmal hemodynamics requires attention to both the aneurysmal morphology and the geometric characteristics of the associated arterial vascular system. The BAtip aneurysms in our series were larger and had deeper domes and wider necks than ICAbif aneurysms. Larger neck sizes lead to higher intra-aneurysmal flow rates and, in combination with the greater depth and volume, have the possibility of greater flow complexity and instability. Why basilar tip aneurysms have larger sizes than ICA aneurysms is unclear. Better understanding of the mechanisms and mechanobiology of aneurysmal growth may prove helpful; however, the perianeurysmal environment may also play an important role in aneurysmal growth because contact with extravascular structures can constrain or influence the aneurysm evolution. Further studies are needed to elucidate the specific contribution of each of these factors and their combined effect on aneurysm progression.

Extending the arguments related to high flow mechanisms contributing to the initiation and progression of cerebral aneurysms can yield insight when applied to the 2 circulations discussed in this study. We chose to compare the ICA bifurcation with the basilar bifurcation because of their analogous anatomy of a T-type bifurcation. Yet, these aneurysms have very different hemodynamics, and
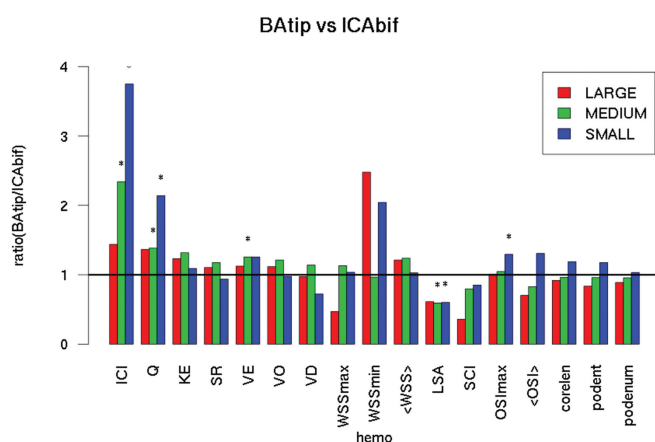
FIG 3. Comparison of hemodynamic variables across BAtip and ICAbif aneurysms grouped according to their sizes as small, medium, and large. KE indicates kinetic energy; SR, shear rate; VO, vorticitiy; VD, viscous dissipation; <WSS>, mean WSS; podent, POD entropy; podenum, POD number of modes; hemo, hemodynamic.
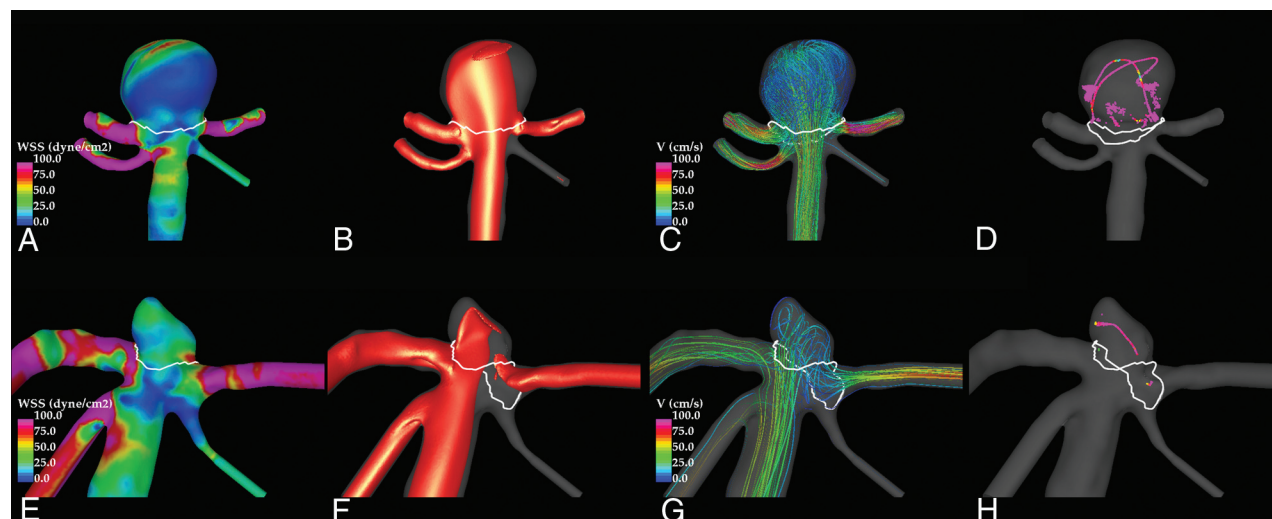
FIG 4. Examples of a ruptured (upper row) and an unruptured (lower row) BAtip aneurysm. Peak systole flow visualizations show the following: wall shear stress distribution (A and E), inflow jet (B and F), flow pattern (C and G), and vortex core lines (D and H). White lines indicate the aneurysm necks.
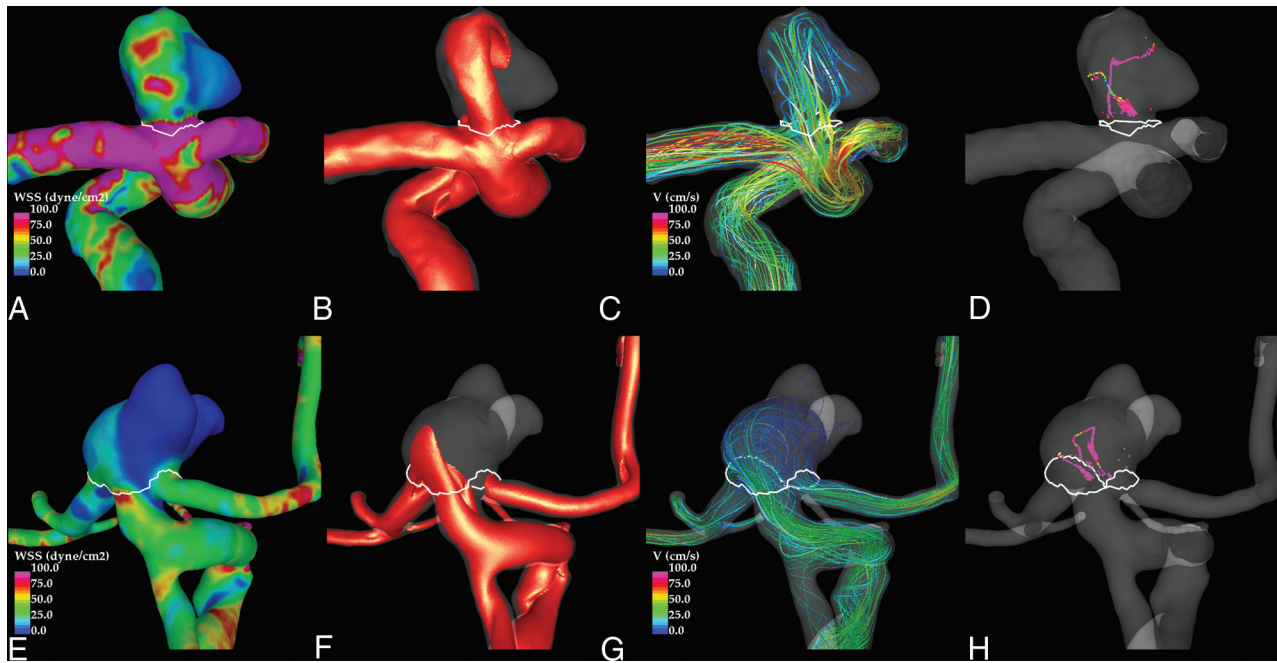
FIG 5. Examples of a ruptured (upper row) and an unruptured (lower row) ICAbif aneurysm. Peak systole flow visualizations show the following: wall shear stress distribution (*A* and *E*), inflow jet (*B* and *F*), flow pattern (*C* and *G*), and vortex core lines (*D* and *H*). *White lines* indicate the aneurysm necks.

a detailed assessment of the parent artery geometry reveals several distinct differences. The artery sizes (both parent and branch arteries) were significantly smaller in the BAtip group along with lower artery tapering compared with the ICAbif group. For a given flow rate, tapering can lead to faster flow velocities and larger pressure drops through an arterial segment, leading to increased WSS within that segment. If this effect occurs proximal to the site of aneurysm formation, then fewer kinetic forces are available for the impaction zone of the flow division where aneurysms are typically located. The tapering of the ICA proximal to the terminus, therefore, may act to reduce the shear at the region of the terminus compared with the basilar artery. Curvature of the proximal ICA can also influence the environment of the terminus. The carotid siphon may cause a consistent deflection of the main flow stream into an impaction in the posterior wall of the supraclinoid ICA, a region of high propensity to aneurysm formation. The curvature of the ICA distal to the posterior communicating artery origin often directs most of the flow stream within the M1 segment, avoiding a direct impaction on the terminus/origin of the A1 segment. In the basilar terminus, this outcome is less often the case with a near-perpendicular impaction and a more equally divided flow stream. Thus, the basilar artery geometry could more often lead to a much higher flow impaction and associated elevated WSS compared with the ICA. Variability of the bifurcation asymmetry and bifurcation angles can lead to further differences in the hemodynamic environments in an individual case. In this sense, ICAbif aneurysms seem to behave more like sidewall aneurysms, while BAtip aneurysms behave more like true bifurcation aneurysms.

Although a number of results reaching statistical significance were identified in this study, some limitations should be considered. The sample size is small when extending into the various subgroups, this could interfere with identifying significant differences. The study was taken from a data base of all aneurysms that had undergone angiography or embolization during a 10-year period. Selection bias related to referral patterns and the indications for treatment may lead to exclusion of an important subset of aneurysms. A number of assumptions were made during the modeling process, including the approximations of the vascular geometry, the inflow conditions, the Newtonian approximation, and the rigid wall assumption.

CONCLUSIONS

High flow conditions, characterized by large and concentrated inflow jets, complex and oscillatory intrasaccular flow patterns, and wall shear stress distributions with focalized regions of high WSS and large regions of low WSS are associated with aneurysm rupture in general and in basilar tip aneurysms in particular. The higher flow conditions in BAtip aneurysms could explain their increased rupture risk compared with ICAbif aneurysms. In ICAbif aneurysms, only trends toward high flow conditions were associated with aneurysm rupture, and these trends were observed in only smaller ICAbif aneurysms. Further studies with larger sample sizes will be needed to determine whether these trends are statistically significant.

ACKNOWLEDGMENTS

REFERENCES

1. Rinkel GJ, Djibuti M, Algra A, et al. **Prevalence and risk of rupture of intracranial aneurysms: a systematic review.** *Stroke* 1998;29:251–56 CrossRef Medline

2. Wiebers DO, Whisnant JP, Huston J 3rd, et al; International Study of Unruptured Intracranial Aneurysms Investigators. **Unruptured intracranial aneurysms: natural history, clinical outcome, and risks of surgical and endovascular treatment.** *Lancet* 2003;362:103–10 Medline

3. Weibers DO, Piepgras DG, Meyer FB, et al. **Pathogenesis, natural history, and treatment of unruptured intracranial aneurysms.** *Mayo Clinic Proc* 2004;79:1572–83 CrossRef Medline

4. Clarke M. **Systematic review of reviews of risk factors for intracranial aneurysms.** *Neuroradiology* 2008;50:653–64 CrossRef Medline

5. van der Kolk NM, Algra A, Rinkel GJ. **Risk of aneurysm rupture at intracranial arterial bifurcations.** *Cerebrovasc Dis* 2010;30:29–35 CrossRef Medline

6. Sforza DM, Putman CM, Cebral JR. **Hemodynamics of cerebral aneurysms.** *Annu Rev Fluid Mech* 2009;41:91–107 CrossRef Medline

7. Higa T, Ujiie H, Kato K, et al. **Basilar artery trunk saccular aneurysms: morphological characteristics and management.** *Neurosurg Rev* 2009;32:181–91; discussion 191 CrossRef Medline

8. Cebral JR, Mut F, Weir J, et al. **Quantitative characterization of the hemodynamic environment in ruptured and unruptured brain aneurysms.** *AJNR Am J Neuroradiol* 2011;32:145–51 CrossRef Medline

9. Yim PJ, Vasbinder GB, Ho VB, et al. **Isosurfaces as deformable models for magnetic resonance angiography.** *IEEE Trans Med Imaging* 2003;22:875–81 CrossRef Medline

10. Taylor CA, Hughes T Jr, Zarins CK. **Finite element modeling of blood flow in arteries.** *Computer Methods in Applied Mechanics and Engineering* 1998;158:155–96 CrossRef

11. Cebral JR, Castro MA, Appanaboyina S, et al. **Efficient pipeline for image-based patient-specific analysis of cerebral aneurysm hemodynamics: technique and sensitivity.** *IEEE Trans Med Imaging* 2005;24:457–67 CrossRef Medline

12. Mut F, Aubry R, Löhner R, et al. **Fast numerical solutions of patient-specific blood flows in 3D arterial systems.** *Int J Numer Method Biomed Eng* 2010;26:73–85 CrossRef Medline

13. Mut F, Löhner R, Chien A, et al. **Computational hemodynamics framework for the analysis of cerebral aneurysms.** *Int J Numer Method Biomed Eng* 2011;27:822–39 CrossRef Medline

14. Byrne G, Mut F, Cebral JR. **Quantifying the large-scale hemodynamics of intracranial aneurysms.** *AJNR Am J Neuroradiol* 2014;35:333–38 CrossRef Medline

15. Tykocki T, Kostkiewicz B. **Aneurysms of the anterior and posterior cerebral circulation: comparison of the morphometric features.** *Acta Neurochir (Wien)* 2014;156:1647–54 CrossRef Medline

16. Wermer MJ, van der Schaaf IC, Algra A, et al. **Risk of rupture of unruptured intracranial aneurysms in relation to patient and aneurysm characteristics: an updated meta-analysis.** *Stroke* 2007;38:1404–10 CrossRef Medline

17. Chien A, Castro MA, Tateshima S, et al. **Quantitative hemodynamic analysis of brain aneurysms at different locations.** *AJNR Am J Neuroradiol* 2009;30:1507–12 CrossRef Medline

18. Robertson AM, Duan X, Aziz KM, et al. **Diversity in the strength and structure of unruptured cerebral aneurysms.** *Ann Biomed Eng* 2015;43:1502–15 CrossRef Medline

19. Cebral JR, Raschi M. **Suggested connections between risk factors of intracranial aneurysms: a review.** *Ann Biomed Eng* 2013;41:1366–83 CrossRef Medline

20. Meng H, Tutino VM, Xiang J, et al. **High WSS or low WSS? Complex interactions of hemodynamics with intracranial aneurysm initiation, growth, and rupture: toward a unifying hypothesis.** *AJNR Am J Neuroradiol* 2014;35:1254–62 CrossRef Medline

21. Can A, Mouminah A, Ho AL, et al. **Effect of vascular anatomy on the formation of basilar tip aneurysms.** *Neurosurgery* 2015;76:62–66; discussion 66 CrossRef Medline

22. Cebral JR, Mut F, Weir J, et al. **Association of hemodynamic characteristics and cerebral aneurysm rupture.** *AJNR Am J Neuroradiol* 2011;32:264–270 CrossRef Medline

23. Dhar S, Tremmel M, Mocco J, et al. **Morphology parameters for intracranial aneurysm rupture risk assessment.** *Neurosurgery* 2008;63:185–197; discussion 196–97 CrossRef Medline

24. Fan J, Wang Y, Liu J, et al. **Morphological-hemodynamic characteristics of intracranial bifurcation mirror aneurysms.** *World Neurosurg* 2015;84:114–20.e2 CrossRef Medline